Contents lists available at ScienceDirect

Molecular Genetics and Metabolism Reports

journal homepage: www.elsevier.com/locate/ymgmr

Generation and characterization of motor neuron progenitors and motor neurons using metachromatic leukodystrophy-induced pluripotent stem cells

Mohammad Arif Hossain [a,b,1,*], Minami Hasegawa-Ogawa [c], Yoko Manome [c], Miki Igarashi [a], Chen Wu [a], Ken Suzuki [a], Junko Igarashi [a], Takeo Iwamoto [a,d], Hirotaka James Okano [c], Yoshikatsu Eto [a,d,*]

[a] *Advanced Clinical Research Center, Institute of Neurological Disorders, Kawasaki, Kanagawa, Japan*
[b] *Department of Gene Therapy, Institute for DNA Medicine, The Jikei University School of Medicine, Tokyo, Japan*
[c] *Division of Regenerative Medicine, The Jikei University School of Medicine, Tokyo, Japan*
[d] *The Jikei University School of Medicine, Japan*

A R T I C L E   I N F O

A B S T R A C T

The pathological consequences leading to primary storage, autophagy impairment, impaired mitochondrial dynamics, and endoplasmic reticulum (ER) stress on neural cell dysfunction and apoptosis in metachromatic leukodystrophy (MLD) have been poorly elucidated. In the present study, we generated 2 cell lines of patient-specific-induced pluripotent stem cells (iPSCs) and modeled the progression of pathological events during the differentiation of iPSCs to motor neuron progenitors (MNPs) and mature motor neurons (MNs). The iPS cells were generated from two late-infantile MLD patient-derived skin fibroblasts using electroporation or the Sendai virus. Olig2$^+$ MNPs were generated from both iPSC lines using a combination of small molecules in a chemically defined neural medium. Furthermore, the MNPs could be differentiated into mature MNs, which was confirmed by RT–PCR and MN markers, including SMI32 and ChAT. The population of MNs was approximately 50% under the culture conditions. Pathological observation of MLD patient-derived iPSCs revealed lysosomal accumulation and impaired autophagy. In addition, both MNPs and MNs derived from MLD-iPSCs showed increased lysosomal accumulation, dysfunctional autophagy, impaired mitophagy, endoplasmic reticulum (ER) stress or unfolded protein response (UPR) activation, and premature cellular death.

1. Introduction

Metachromatic leukodystrophy (MLD) is a rare lysosomal storage disorder (LSD) caused by a deficiency of arylsulfatase A (ARSA; EC 3.1.6.8). ARSA catalyzes the desulfation of 3-O-sulfogalactosylceramide (sulfatide) [1], a sphingolipid that plays key roles in the development and function of myelin-forming cells as well as in the organization and maintenance of myelin structure [2–5]. Abnormal accumulation of sulfatide in white matter and peripheral nerve tissues triggers pathological inflammatory responses in glia and brain-resident immune cells and significantly induces the production of various inflammatory mediators, leading to progressive demyelination and dysfunction of motor neurons

of the central and peripheral nervous systems. A typical late-infantile forms of MLD proceeds to rapid motor and cognitive decline and early death, while juvenile or adult forms display a slower progression of motor symptoms and are sometimes associated with cognitive and behavioral problems [6–8]. The accumulation of sulfatide also shows abnormal neuronal cell morphology and organization, leading to axonal degeneration [9,10] and contributing to motor dysfunction in MLD patients [11]. Furthermore, the MLD brain pathologically exhibits gray matter astrogliosis, which leads to axonal involvement [12,13]. Mitochondria and ER form structural and functional networks (mitochondria-associated ER membranes are essential for maintaining cellular homeostasis and determining cell fate under various pathophysiological
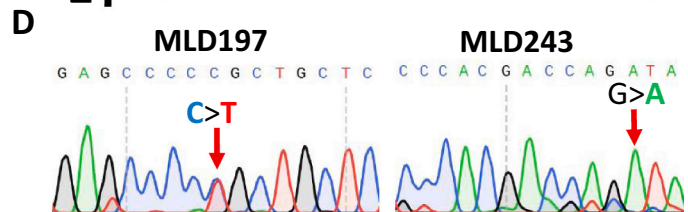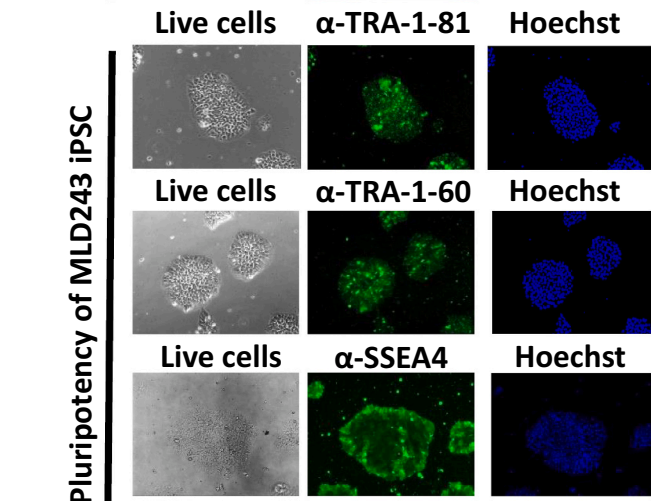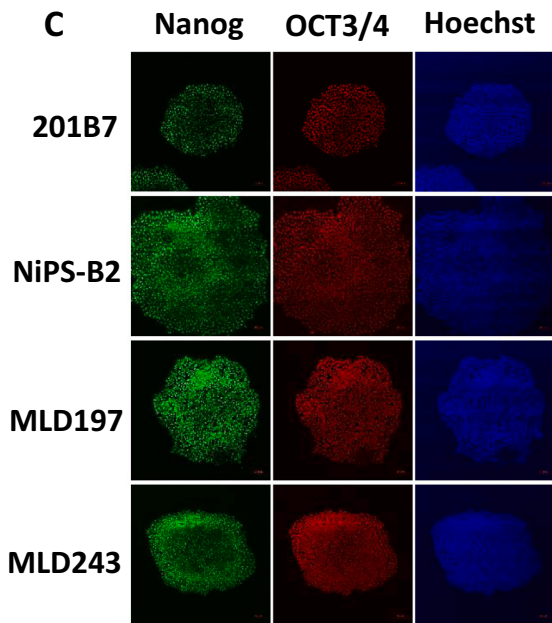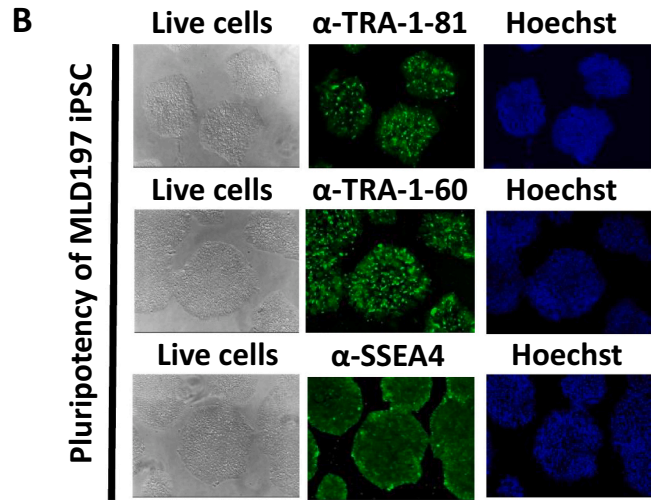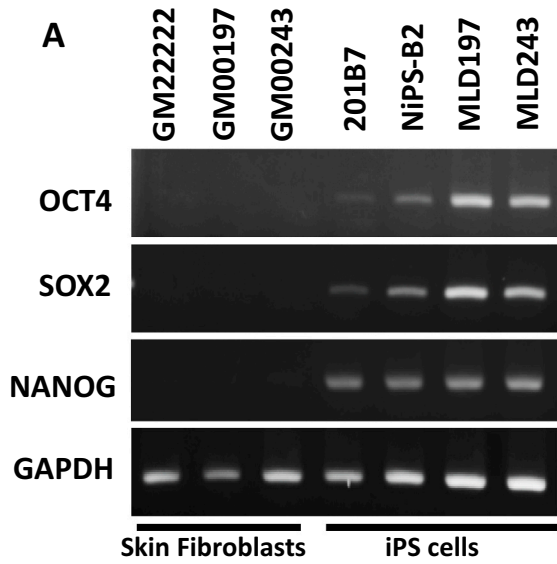
(caption on next page)

Fig. 1. Human iPS cells derived from normal healthy controls and MLD patients and their characterization. A. RT–PCR analysis of *OCT4*, *SOX2* and *NANOG* for the confirmation of pluripotency of iPS cells. cDNA was derived from SFs of healthy subject GM22222 and two patients with late-infantile MLD, GM00197 and GM00243 for the first three lanes as a negative control, and RT–PCR was performed. The fourth to seventh lanes are iPS cells from normal controls (201B7, NiPS-B2) and patient SF-derived iPS cells. *GAPDH* was used as a loading control. B and C. Immunostaining for pluripotency markers. Pluripotency was confirmed by anti-α-TRA-1-81, α-TRA-1-60 and α-SSEA4 for the iPS cells generated in this study. Anti-OCT3/4 and anti-NANOG antibodies were used to confirm the pluripotency of all iPS cells used in this study. Hoechst was used for nuclear DNA staining. D. Mutation analysis of the *ARSA* gene of patients with MLD. Genomic DNA was extracted from SFs and iPS cells, and direct sequencing was performed. A single base nucleotide change, c.1277C > T, was detected in GM00197 SFs and their derived iPS cells in the heterozygous state, which caused one amino acid change, p. P426 L. A homozygous intronic mutation c.459 + 1G > A (CAGgta>CAGata) is detected in GM00243 SFs and their derived iPS cells. Both mutations were reported as common in Caucasian people. E. Chromosomal karyotyping. Twenty cells from colonies #3 of MLD197 and #9 of MLD243 were checked and showed a normal 46, XY chromosomal pattern.

conditions). Regulated Ca^{2+} transfer from the ER to the mitochondria is important for maintaining the control of prosurvival/prodeath pathways [14]. The generation of patient-specific induced pluripotent stem cells (iPSCs) and their differentiation into progenitor or mature neuronal cells could be applied for human disease modeling and therapeutic approaches [15–18]. LMD patient-specific iPSCs have been differentiated into neural progenitors for therapeutic potential [19–21]. However, these different pathogenic mechanisms in MLD have not been studied in neurons and associated cells. We generated iPSCs from skin fibroblasts of two late-infantile MLD types and then differentiated them into motor neuron progenitors (MNPs) and motor neurons (MNs). We studied the phenotypic expression of these MNPs and MNs by analyzing intracellular biochemical abnormalities, including ER stress, autophagy, mitophagy, and cellular apoptosis, by RT–PCR, immunostaining, and electron microscopy.

2. Materials and methods

2.1. Fibroblasts and clinical phenotypes

Skin fibroblasts (SFs) were purchased from the Coriell Institute for Medical Research; one healthy subject, GM22222 (age at sampling: 1 day), and two MLD patients, GM00197 and GM00243. GM00197 was established from a 4-year-old male Caucasian who had late-infantile onset MLD. His phenotype was described as significantly increased sulfatide excretion in urine, deficient in arylsulfatase A and having two similarly affected siblings from unaffected parents [22]. GM002434 was established from a 3-year-old male Caucasian who had late-infantile onset MLD. No genotype information was described previously. SFs were cultured in a humidified 5% CO2 incubator at 37 °C in Dulbecco's modified Eagle's medium (DMEM; SIGMA) supplemented with 10% fetal bovine serum (FBS; Life Technologies/Gibco) and 1% penicillin/streptomycin (SIGMA).

2.2. Normal iPS cell lines

The human iPSC Lines 201B7 and Nips-B2 were used as healthy control iPSC lines. Basic information on the origin of these human iPSCs, including medical history, sex, age, tissue, reprogramming factors, and vector type, were summarized in our recent article [23]. The iPS cell lines, including the lines generated in this study (see below), were maintained on 35 mm dishes with StemFit AK02N medium (Ajinomoto, Tokyo, Japan) as previously described [23].

2.3. Generation of iPS cells from fibroblasts of MLD patients

GM00197 (MLD197) iPSCs were generated from human dermal fibroblasts (HDFs) using episomal vectors according to a protocol from CiRA (Center for iPS Cell Research and Application, Kyoto University) [24]. Using an Amaxa Nucleofector HDFs kit (Lonza VAPD-1001), electroporation was performed with the gene transfer device Nucleofector I. The episomal vectors (OCT3/4, SOX2, KLF4, L-MYC, LIN28, p53-shRNA) pCXLE-hOCT3/4-shp53-F, pCXLE-hSK and pCXLE-hUL) obtained from Addgene harboring reprogramming factors were then transferred to generate iPSCs (Fig. S1A). GM00243 (MLD243) iPSCs

were generated from HDFs using the Sendai virus (SeVdp) vector according to the protocol described by Nishimura et al. [25]. The SeVdp vector simultaneously delivered four Yamanaka factors (Klf4, Oct4, Sox2, and c-Myc) and the siRNA L527 (5-GGUUCAGCAU CAAAUAUGAAG-3,3-UACCAAGUCGUAGUUUAUACU-5) (Fig. S1B). iPSCs were generated, supplied, and preserved on feeder cells and mouse embryonic fibroblasts. Later, they were cultured under feeder-free conditions [23,26].

### 2.4. Mutation analysis and karyotyping

Genomic DNA was extracted from patient-derived SFs and iPSCs, and all eight exons and adjacent introns were amplified by PCR using three sets of primers (Table S1) for the *ARSA* gene. The amplified fragments were then purified and sequenced by Eurofins Genomics K.K. Japan. Karyotyping was performed for the iPSCs generated by Nihon Gene Research Laboratories Inc. (contract analysis).

2.5. Generation of neuroprogenitor cells or motor neuron progenitors

Neurospheres were generated as a source of neuroprogenitor cells (NPCs), as reported previously [27] with a mild modification. In short, approximately $4–5 \times 10^5$ iPSCs were passaged in a 35-mm dish with StemFit AK02N medium and maintained until they reached 50% confluence as an adherent culture. When the size of the cell colonies was >1 mm, preinduction of NPCs was introduced by 3 μM CHIR99021 (CAYMAN, cat. 13,122), 3 μM SB431542 (Sigma, cat. S4317-5MG, hydrate), and 3 μM dorsomorphin (Santa Cruz, SC-200689) with StemFit AK02N medium for 5 days at 37 °C in a 5% CO$_2$ incubator. The cells were then peeled with TrypLE Select (diluted to 0.5×, GIBCO), and the dissociated cells were then cultured in suspension with Kohjin Bio Medium (KBM) (KOHJIN BIO, cat. 16,050,100) containing 2% vitamin B27 (Gibco, cat. 17,504–044), 10 ng/ml recombinant human leukemia inhibitory factor (Merck Millipore, cat. LIF1010), 10 mM Y27632 (FUJIFILM Wako Chemicals, cat. 251–00514), 2 ng/ml basic fibroblast growth factor (FUJIFILM Wako Chemicals, cat. 060–04543), 2 μM SB431542 (Sigma, cat. S4317), 3 μM CHIR99021 (Cayman, cat. 13,122), 10 ng/ml retinoic acid (FUJIFILM Wako Chemicals, cat. 182–01116), and 1 μM purmorphamine (Cayman, cat. 10,009,634). The suspended cells (NS0) were incubated at 37 °C in a 5% CO$_2$ and 4% O$_2$ incubator for 6–7 days. Subculture or preservation in liquid nitrogen was considered when the sphere size was between 70 and 150 μm. For analysis of NPCs, the neurospheres (NS1) were passaged once with the same culture medium until the size of the neurospheres was 300–1000 μM. NS1 would then either be used for MN induction or for NPC adherent culture. Olig2-positive NPCs were considered MNPs. Cell pellets from NS1 were also used for RNA extraction or ARSA activity measurement.

2.6. Generation of motor neurons

Suspended NPCs (NS1) were used for MN induction as described previously [28], with minor modifications. In short, mature neurospheres (>300 μM) were treated with TrypLE Select to make single-cell suspensions, count the cell number, and start adherent culturing in KBM with micronutrient-specific supplements. The supplements included 2%
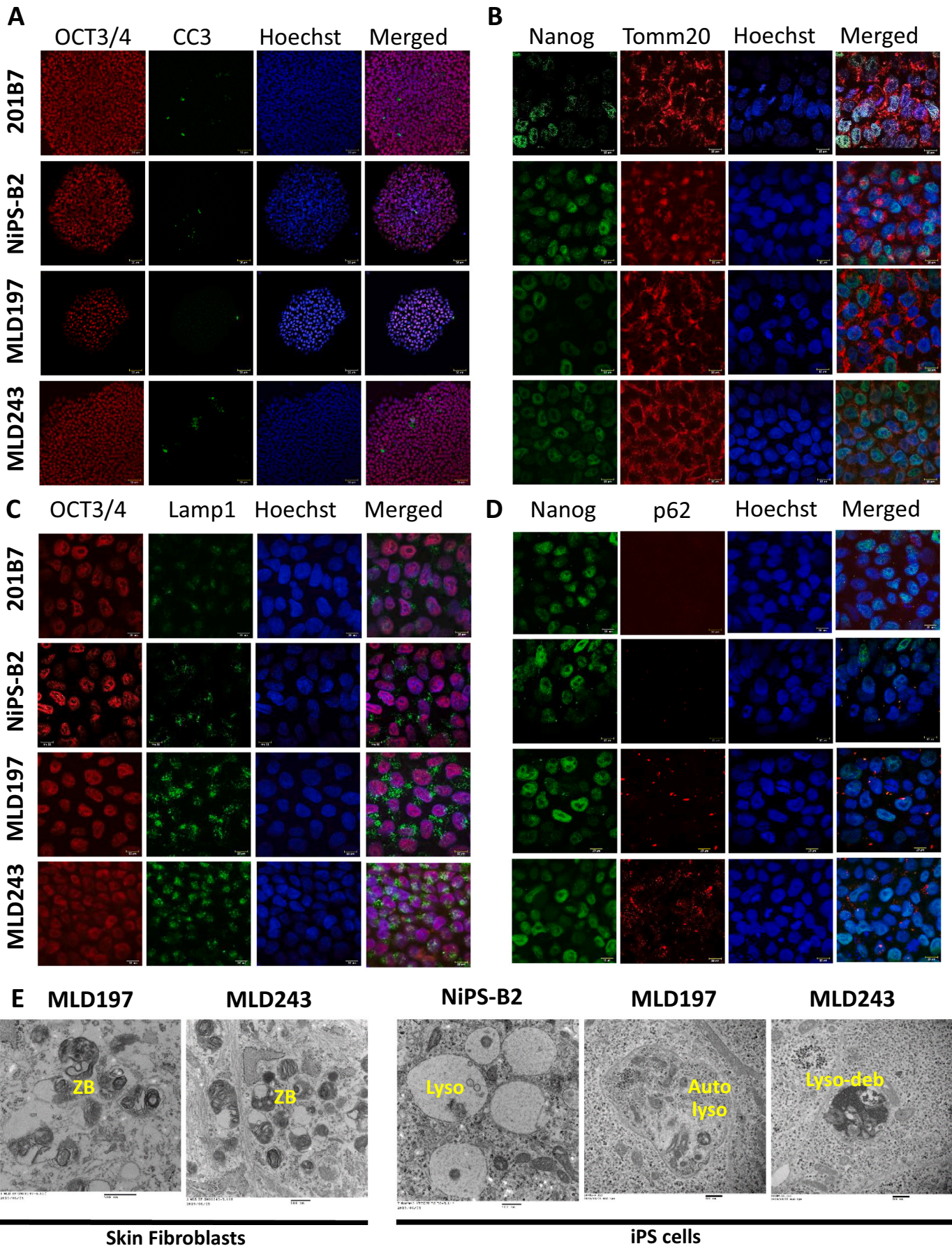
Fig. 2. Morphological and pathological characteristics of iPS cells. A. Detection of apoptotic cells by cleaved caspase 3 (CC3). No significant abnormalities were detected between normal and patient-derived iPS cells with respect to pluripotency by OCT3/4 or by the number of CC3-positive cells. B. Mitochondrial morphology. Mitochondrial morphology was detected by an antibody against the mitochondrial outer membrane protein TOMM20, and it showed no differences between normal and patient-derived iPS cells. C. Detection of lysosomes. Patient-derived iPS cells show enhanced LAMP1 both in the size of the lysosomes and the area of each cell. D. Observation of autophagy/mitophagy. Aberrant p62/SQSTM1 accumulation is observed in iPS cells derived from MLD patients. E. Electron microscopy. Electron microscopy of SFs from both MLD patients shows massive lysosomal deposits manifested as Zebra Bodies (ZB). Few lysosomal deposits (lyso-deb) and autolysosomes (autolyso) with immature membranes are observed in patient-derived iPS cells.

vitamin B27, 1% N2 (Gibco, cat. 17,502–048), 10 ng/ml recombinant human brain-derived neurotrophic factor (BDNF) (R&D system, cat. 248-BD), 10 ng/ml recombinant human glial cell line-derived neurotrophic factor (GDNF) (R&D system, cat. 212-GD), 50 ng/ml small molecule recombinant human Sonic Hedgehog (hSHH) (R&D system, cat. 1845-SH), 200 ng/ml ascorbic acid (Wako chemicals, cat. 012–04802), 1 mM dibutyl cyclic AMP (Sigma–Aldrich, cat. D0627), 10 ng/ml recombinant human insulin-like growth factor-1 (R&D system, cat. 291-G1), and 50 nM retinoic acid (Wako chemicals, cat, 182–01116). The cells were seeded on poly-L-ornithine (Sigma–Aldrich, cat. P3655) and laminin (Invitrogen, cat. 23,017–015)-coated cell desk LF1 (Sumilon, cat, MS92132) or culture plates. The culture medium was changed with the same medium on alternate days. When the color of the medium was altered in one day, the medium was changed every day until 4 weeks (28 days) of culture.

2.7. ARSA activity measurement

For ARSA activity, total cell lysates from SFs, iPSCs, or NPCs (NS1) were incubated with 4-MU sulfate potassium salt with or without $AgNO_3$ as described previously [29]. After 2 h of incubation at 37 °C, the reactions were stopped with 150 mM ethylenediaminetetraacetic acid (EDTA; pH 11.5) buffer. Fluorescence (excitation at 355 nm/emission at 460 nm) was measured using a microplate reader (ARVO (TM) X3, Perkin Elmer, USA). ARSA activity was calculated as total ARS activity minus AgNO3 inhibited activity. The enzyme activity was calculated as $nmol·h^{-1}·mg$ $protein^{-}$

2.8. RT–PCR and quantitative PCR

Total RNA was extracted from iPSCs, NPCs, and differentiated MNs using an RNeasy Plus Mini Kit (Qiagen; Ref. 74,104) following the manufacturer's instructions. cDNA was synthesized from extracted total RNA using a ReverTra Ace® qPCR RT Master Mix with gDNA Remover (Toyobo, Ref. FSQ-301). RT–PCR was performed using GoTaq® Master Mixes (Promega, cat. M7122). Quantitative PCR (qPCR) was performed using an Mx3000p qPCR system (Agilent, USA) with PowerUp SYBR Green Master Mix (Thermo Fisher Scientific, cat. A25742) following the manufacturer's protocol. The expression level of each gene was calculated using the comparative cycle threshold method, and the mRNA levels of target genes were normalized using the mRNA expression of *β-actin* as the housekeeping gene. The primer sets used for RT–PCR and qPCR are listed in Table S2.

2.9. Electron microscopy

Transmission electron microscopy (TEM) was performed using an H-7500 (Hitachi, Japan) for iPSCs, NPCs, and differentiated MNs per our published article [23]. Scanning electron microscopy (SEM) was conducted only for differentiated MNs. Briefly, cells were fixed in 1% glutaraldehyde and 0.1 M phosphate buffer (pH 7.4). The fixed cells were treated with 0.1% aqueous tannic acid and 0.2% aqueous uranyl acetate. After rinsing with distilled water, the cells were dehydrated in two steps: an ascending ethanol series and a high concentration of hexamethyldisilazane (HMDS). All SEM images were obtained using Regulus 8100 (Hitachi, Japan) in the high vacuum mode.

2.10. Immunocytochemistry

Cells, including iPSCs, MNPs, and MNs, were cultured on a cell desk LF1 (Fujifilm) for immunocytochemistry (ICC). The cells were then fixed with 4% paraformaldehyde (PFA) for 15 min at room temperature. Cellular permeabilization was performed in 0.5% Triton X for 15 min. Blocking of nonspecific proteins was performed in 5% BSA or 5% goat serum and 0.3% Triton X in PBS for 1 h at room temperature. Cells were then incubated with primary antibodies for marker proteins indicating iPSCs, MNPs, MNs, and organelle markers overnight at 4 °C. Alexa 488, 555, 633, and 647 secondary antibodies were used for counterstaining for 1 h at room temperature. Hoechst 33342 was used as a nuclear stain. The names of the antibodies, target cells/organelles, host species and their concentrations are listed in Table S3. A Zeiss LSM-880 confocal laser-scanning microscope was used to obtain the original image of cells at 20× magnification. A 100× magnification was used to visualize the cell organelles, including the mitochondria, lysosomes, and p62. ImageJ software (https://imagej.nih.gov/ij/download.html) was used to analyze the number of cells. First, the original images (20×) were converted into 16-bit images, and the brightness, contrast, and threshold were adjusted to ensure that all cell nuclei and CC3- and/or SMI32-positive cells were visible.

2.11. Statistical analysis

Experiments were performed at least three times. Data are presented as the mean ± standard error (SEM). Statistical significance was evaluated by one-way analysis of variance or an unpaired Student's *t*-test, as appropriate. Post hoc analyses were conducted using Dunnett's multiple comparison test, as appropriate, to compare means when significant differences were identified. The results were considered statistically significant at $p < 0.05$.

3. Results

3.1. Analysis of iPS cells

3.1.1. Generation of iPS cells and their pluripotency

iPSCs were generated from two fibroblasts, GM00197 and GM00243, derived from MLD patients by electroporation and Sendai virus, respectively. We decided to use colony #3 from GM00197 as MLD197 and colony #9 from GM00243 as MLD243 for further experiments because of their normal chromosomal karyotypes (Fig. 1E). These cells were stained with α-TRA-1-81, α-TRA-1-60 and a-SSE4 (Fig. 1B), indicating their pluripotency. In addition, OCT4, SOX2, and NANOG mRNAs were expressed in the generated iPSCs as well as normal iPSCs, NipsB2 and 201B7, but not original fibroblasts (Fig. 1A). Furthermore, OCT4 and NANOG proteins were detected in the iPSCs generated as wells as normal iPSCs by ICC (Fig. 1C).

3.1.2. ARSA gene analysis

A C > G nucleotide changing threonine at position 391 to serine in the heterozygous state (p. T391S) (data not shown) in the GM00197 cell lines was reported as a polymorphism previously [22b]. A heterozygous mutation p. P426 L detected in the GM00197 cell lines was reported as a pathogenic variant [22c]. The two alleles could not be detected
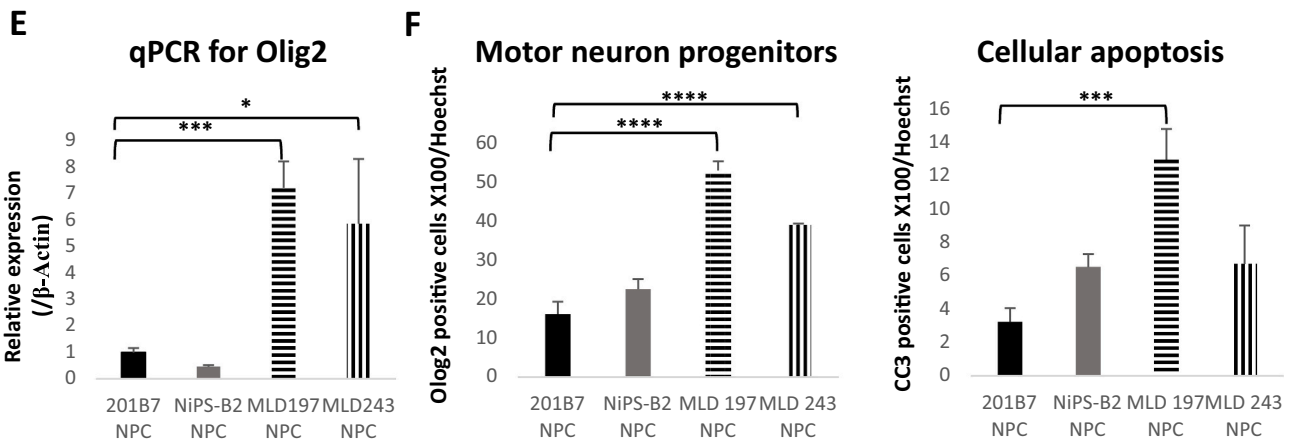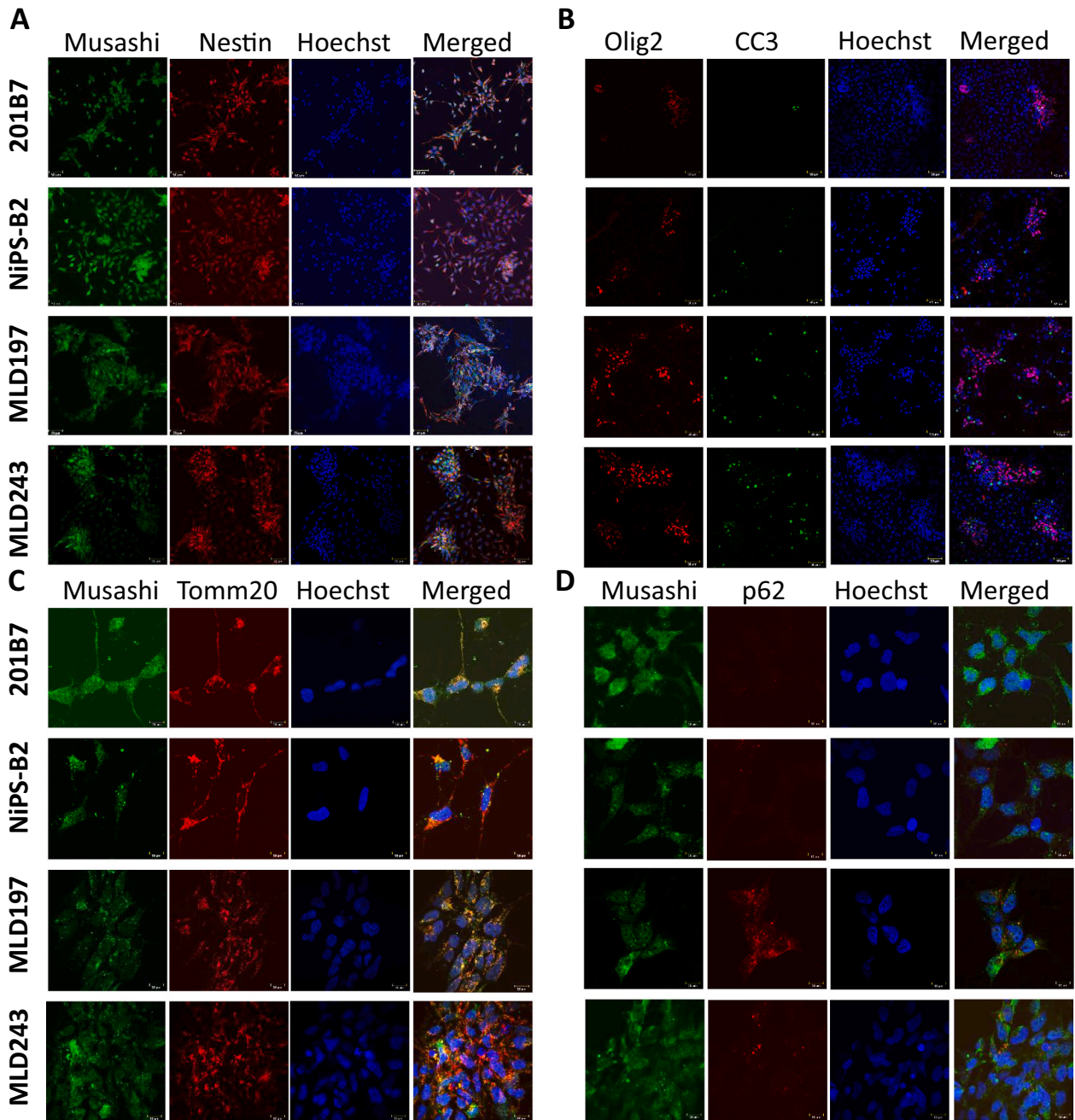
(caption on next page)

Fig. 3. Morphological and pathological characteristics of NPCs. A. Multipotency of neuroprogenitor cells. Nestin and musashi were used to confirm the multipotency of NPCs, and they appear to have similar expression in normal and patient-derived NPCs. B. Detection of MNPs and apoptotic cells. MNPs were detected by Olig2, and the number was found to be significantly high in patient-derived NPCs. CC3-positive NPCs were also detected in a high ratio. The cell number is calculated in Fig. F. Expression of Olig2 by qPCR is also detected in a high ratio in Fig. E. C. State of mitochondria. Aggregated and fragmented mitochondria were found to accumulate around NPC nuclei derived from patients. D. Observation of autophagy/mitophagy. Aberrant p62/SQSTM1 accumulation is observed in patient-derived NPCs. Each bar represents the mean ± SEM of three determinations. *$p < 0.05$, **$p < 0.01$, ***$p < 0.005$ and ****$p < 0.0001$.

individually, and the second mutation was not unveiled [22c]. A homozygous c.459 + 1G > A (CAGgta>CAGata) mutation was detected in GM00243 cell lines. The mutations were consistent with both the DNA of SFs and iPS cells (Fig. 1D).

3.1.3. ARSA activity

ARSA activity was measured in both SFs and iPSCs to evaluate the expression of ARSA in the developmental period. The ARSA activity in SFs for healthy subjects was 18–20 nmol·h^{-1}·mg protein^{-1}, while the MLD patients had very low or no ARSA activity. For iPSCs and NPCs, the ARSA activity was low even for healthy subjects (Fig. 4E).

3.1.4. Electron microscopy

TEM of SFs and iPSCs from both MLD patients was performed. Massive lysosomal depositions were observed in both patients' SFs, presented as zebra bodies (ZB); however, few depositions were observed in their iPSCs (Fig. 2E). Some autolysososmes with immature membranes were observed in the patients' iPSCs.

3.1.5. Morphological and pathological characteristics of iPS cells

To observe the pathophysiology of MLD patient-derived iPSCs, the cells were stained with lysosome marker (LAMP1) (Fig. 2C), mitochondrial marker (TOMM20) (Fig. 2B), apoptosis marker cleaved caspase 3 (CC3) (Fig. 2A), and autophagy/mitophagy marker (p62/SQSTM1) (Fig. 2D) as primary antibodies. There were no significant differences between normal subjects and the patients' iPSCs in terms of TOMM20 and CC3 expression. However, LAMP1 expression seemed to be enhanced in iPSCs compared to normal iPSCs, indicating lysosomal deposition. In addition, aberrant p62/SQSTM1 accumulation was confirmed in iPSCs derived from MLD patients, indicating impaired autophagy and mitophagy. Next, we analyzed the mRNA expression levels of marker genes related to ER stress, including activating transcription Factor 4 (ATF4), activating transcription Factor 6 (ATF6), binding immunoglobulin protein (BiP/GRP-78), homocysteine-responsive endoplasmic reticulum-resident ubiquitin-like domain member 1 (HERPUD1), and the C/EBP homologous protein (CHOP) transcription factor. In addition, the expression of mitochondrial dynamics and mitophagy-related proteins, including dynamin-related protein 1 (Drp1), mitochondrial fission 1 protein (FIS1), mitochondrial fission factor (MFF), dynamin-like 120 kDa protein (OPA1), mitofusins (Mfn1), and mitofusins (Mfn2), was also examined. We could not detect any significant difference in the mRNA expression of ER stress-related proteins between normal cells and iPSCs derived from patients (Fig. S2). However, the expression of the mitophagy-related protein Drp1 was significantly reduced in both MLD197 and MLD243 iPS cells, and Mfn2 and OPA1 were reduced in MLD243 iPSCs (Fig. S2).

3.2. Analysis of motor neuron progenitors

3.2.1. Generation of NPCs and their pluripotency

Four iPSC lines cultured to generate NPCs were subjected to ICC to characterize their morphological and pathological features. All the cells were observed to be positive for nestin and musashi, pluripotency markers for NPCs, without any difference between patients and normal cell lines (Fig. 3A). Interestingly, the number of Olig2-positive cells, which would be considered MNPs, was significantly higher for patient-derived NPCs (Fig. 3B, F), while Olig2 expression by qPCR was also remarkably high (Fig. 3E).

3.2.2. Electron microscopy

TEM revealed elongated and tubular mitochondria distributed throughout normal NPCs. However, very few elongated mitochondria were observed primarily in the periphery of the patient's NPCs. Short, fragmented mitochondria accumulated around the surrounding nuclei of the MLD-derived NPCs. This indicated that mitochondrial fission was induced and that unhealthy fragmented mitochondria had lost this dynamic. A few autolysosomes and ZB were observed in the patients' NPCs. Mild endoplasmic dilatation was observed in the MLD197-derived NPCs (Fig. 4B).
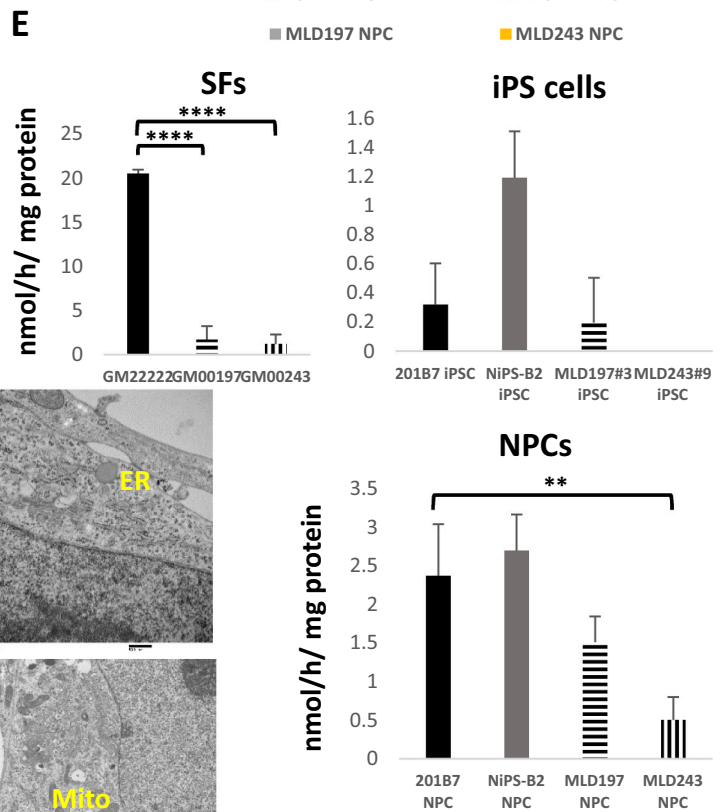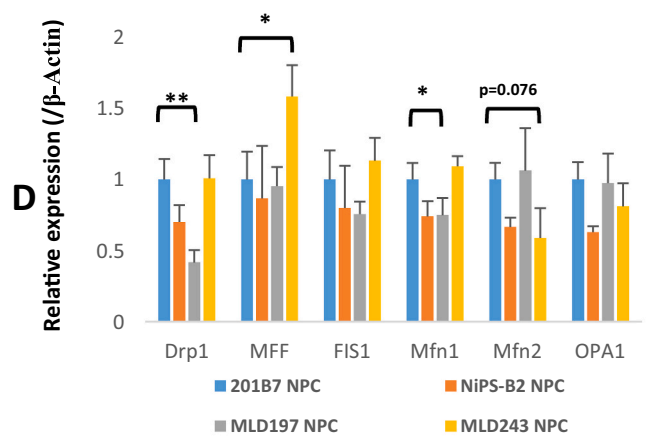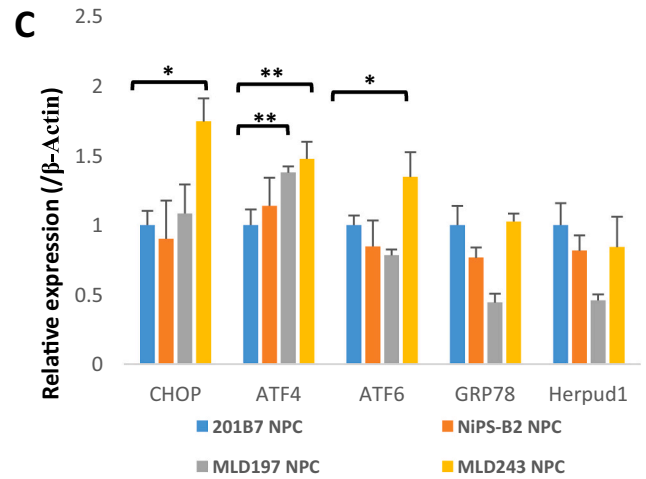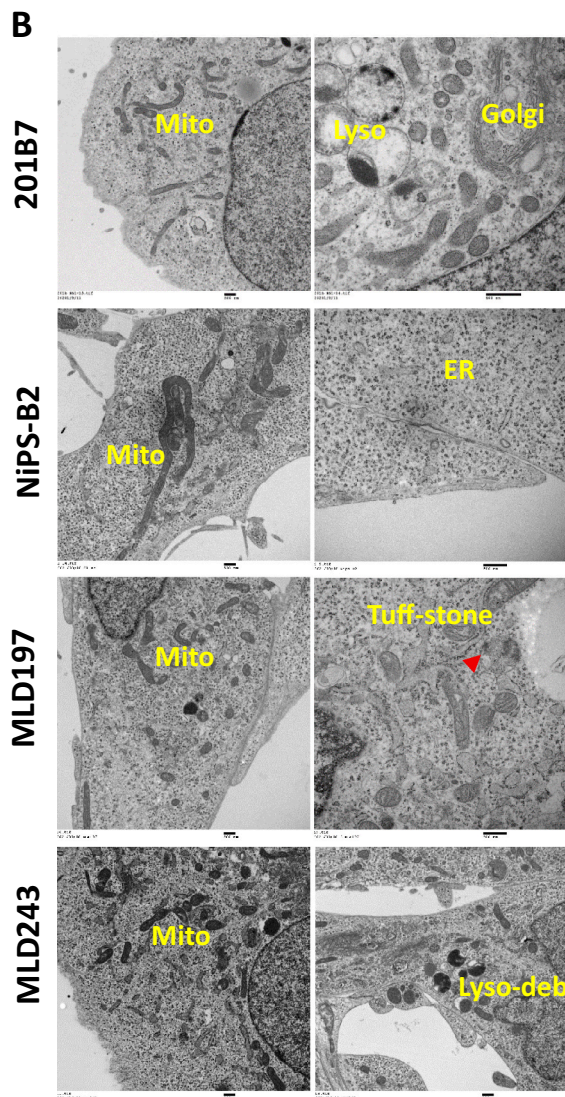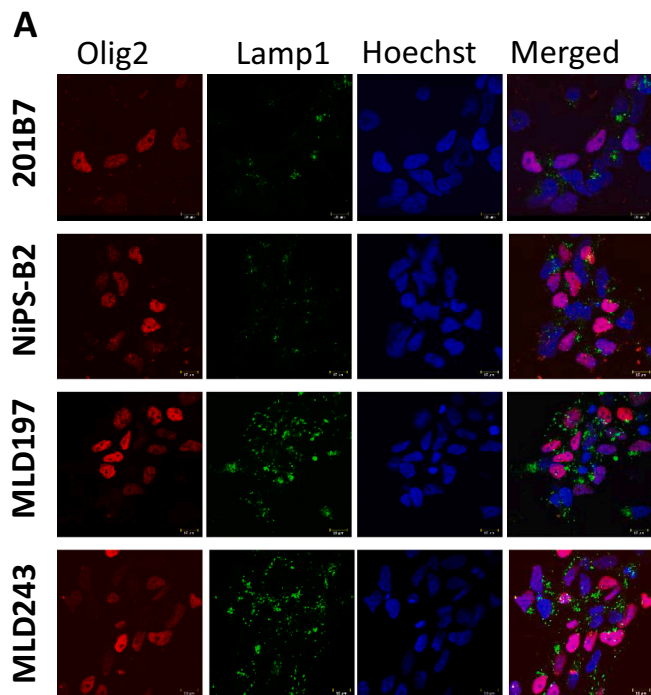
3.2.3. Morphological and pathological characteristics of NPCs

To observe the pathophysiology of MLD patient-derived NPCs, the cells were stained with primary antibodies against CC3, LAMP1, TOMM20, and p62/SQSTM1. A significant number of CC3-positive cells were observed in MLD patient-derived NPCs (Fig. 3B, F). Aggregated and fragmented mitochondria accumulated around the patient's cell nuclei (Fig. 3C). Remarkable LAMP1 and p62/SQSTM1 aggregation was also observed in the patient-derived NPCs (Fig. 4A, 3D). qPCR for ER stress proteins revealed high expression of CHOP, ATF4, and ATF6 in the patient-derived NPCs (Fig. 4C), which signified UPR activation. Mitochondrial dynamics and mitophagy-related proteins showed downregulated levels of Drp1, Mfn1 and Mfn2 and upregulated levels of MFF (Fig. 4D), indicating impaired mitophagy and mitochondrial dynamics.

3.3. Analysis of differentiated neuronal cells

3.3.1. Neuronal differentiation and maturation

To confirm the differentiation of neurons and associated cells, the cells were stained with antibodies against marker proteins for various neuron-associated antibodies, including Tuj1 for neurites, Map2 for mature neurons, SMI32 and ChAT for mature motor neurons, GFAP for mature astrocytes, and O1 for mature oligodendrocytes. Under the differentiated conditions used in this study, we detected several types of cells, including neurons, astrocytes, undifferentiated NPCs, and some noncategorized cells, in the culture population. Based on the counting results, approximately 50% of cells were differentiated into mature neurons (Map2 positive) and motor neurons (SMI32 positive) (Fig. 5A, B) in all cell lines, indicating that most of the neurons in the culture were motor neurons. However, MLD243 showed fewer differentiated cell populations by ICC (Fig. 5A, C) and weak expression of Tuj1, Map2 and ChAT by qPCR (5E). Differentiation to astrocytes revealed significant impairment in both MLD197 and MLD243 (Fig. 5D, E). We could not find any oligodendrocytes by ICC in the culture using our current experimental methods (data not shown). Notably, Olig2-positive undifferentiated MNPs were largely detected in the patient cell population (Fig. 6A).

(caption on next page)

Fig. 4. Pathological characteristics of the NPCs. A. Detection of lysosomes. Patient-derived NPCs show enhanced LAMP1 both in the size of the lysosomes and the area of each cell. B. Electron microscopy. Different types, including long, short and even mitochondrial fusion, are observed throughout the cells in normal NPCs. However, patient-derived cells show mostly fragmented mitochondria around the nucleus. The lysosomes are also filled with tuff-stone inclusions or lysosomal debris in patient-derived NPCs. ER was also found to be dilated in MLD197 NPCs. C. ER stress-related mRNA expression by qPCR. D. Mitochondrial dynamics and related mRNA expression. E. ARSA activity in SFs, iPS cells and NPCs. Each bar represents the mean ± SEM of three determinations. $*p < 0.05$, $**p < 0.01$, $***p < 0.005$ and $****p < 0.0001$.

3.3.2. Electron microscopy

SEM was performed for mature neurons in the culture at 28 days, and no morphological changes were observed between patients and controls (Fig. 6E). TEM revealed large lysosomal tuff stone inclusions and ZB in the patient-derived neurons. In patient-derived neurons, mitochondria were mostly fragmented and deposited around the nucleus. The endoplasmic reticulum was found to be largely engorged in patient neurons only (Fig. 6F).

3.3.3. Morphological and pathological characteristics of differentiated neurons

For the observation of neuropathology of the neuronal cells, the cells were stained with antibodies against CC3 for cellular apoptosis, LAMP1 for lysosomes, TOMM20 for mitochondria, and p62/SQSTM1 for autophagy/mitophagy. Many CC3-positive cells were observed in the culture of patient-derived cells. The percentage of positive cells was approximately 22–25% in the cultures of patient-derived cells, while it was approximately 5–8% in the cultures of normal cells (Fig. 5A, B). Lysosomes were found to have remarkable enhancement (Fig. 6D), and p62/SQSTM1 aggregation was observed in the patient-derived neurons (Fig. 6C). Patient-derived neuronal mitochondria were also found to be largely fragmented and centrally aggregated (Fig. 6B).

4. Discussion

A human disease model is required to describe the pathophysiology of the disease and the progression of CNS pathology of neurodegenerative LSDs. Human iPSC-derived neurons have been used as a model system of the neuronal defects of several LSDs, including mucopolysaccharidosis [30–32], Niemann−Pick type C [23], Gaucher disease [33–36], GM1 gangliosides [37], NCL [38], and MLD [19–21]. Since loss of motor skills (such as walking, moving, speaking, and swallowing), stiff and/or rigid muscles, poor muscle function, and paralysis are the main phenotypes expressed by the affected cases of MLD, we generated iPSCs from MLD patient-derived fibroblasts and differentiated them into MNPs (NPCs) and MNs. Although the culture conditions should be re-evaluated to pure MNs from iPSCs, we produced MLD patient-derived MNs that could be an addition to previous studies describing human iPSC-based models of LSDs.

In several LSDs, including GM1-gangliosidosis, neural ceroid lipofuscinosis, Tay–Sachs disease, and Gaucher disease, the unfolded protein response or ER stress pathway is thought to play a vital role in their pathophysiology [39–43]. Considering that major structural alterations in the ER and Golgi complex, the accumulation of storage vacuoles, and increased apoptosis were observed both at the protein expression and ultrastructural levels in MPS II neuronal cells, it was hypothesized that lysosomal membrane protein carrier vesicles have an initiating role in the formation of storage vacuoles, leading to impaired lysosomal function [44]. We also reported a UPR response in globoid leukodystrophy or Krabbe disease and upregulation of GRP78/BiP [45]. In this study, we detected the upregulation of CHOP, ATF4, and ATF6, which led to ER stress, lysosomal accumulation, impaired autophagy-mitophagy (Figs. 2–6) and consequently worsened cellular differentiation and

ultimately led to premature cell death in patient-derived MNPs (Fig. 3B, F) and MNs (Fig. 5A, B).

The mitochondrial proteins Drp1, FIS1, and MFF mainly participate in mitochondrial fission, while OPA1, Mfn1, and Mfn2 are the main components of mitochondrial fusion. Furthermore, Drp1, Mfn1, and Mfn2 play a major role in mitophagy [46]. Additionally, Drp1 deficiency causes mitochondrial dysfunction and neurotoxicity [47]. In MLD-derived iPSCs generated in this study, we detected reduced synthesis of Drp1 and Mfn2 (Fig. S2), which led to impaired mitophagy (Fig. 2D). Additionally, overexpression of MFF in MLD-derived NPCs (Fig. 4D) triggers mitochondrial fission, manifested by the aggregation of fragmented mitochondria around the nucleus (Fig. 3C, D, 4B), which might enhance cellular apoptosis [48]. The aggregation of fragmented mitochondria around the nucleus can also be explained by the loss of mitochondrial dynamics. Similar effects were observed in patient-derived MNs (Fig. 6B, C).

Olig2-positive NPCs, which are recognized as MNPs, have been described as the main source of motor neuron and oligodendrocyte differentiation [49,50]. It has also been reported that chronic neuronal damage induces overexpression of Olig2 and overgrowth of MNPs [51]. Our current study revealed similar data, showing overexpression of Olig2 and overgrowth of MNPs due to the early death of many neural cells (Fig. 3B, E, F). Even after four weeks of differentiation, Olig2-positive MNPs were still present in the patient cell population (Fig. 6A) in response to cellular death [51]. Although we could not measure sulfatide accumulation, it may influence cellular death [20–21].

Astrocytes are an essential cell type for neural development, including synapse formation and axon myelination, as well as for ensuring homeostasis of the CNS [52]. In many neurodegenerative diseases, such as Alzheimer's, Parkinson's, and amyotrophic lateral sclerosis, the number and function of astrocytes are lost. Moreover, the loss of astrocytes may also lead to the loss of oligodendrocyte integrity [53]. Although we could not differentiate oligodendrocytes in our study, we found that the differentiation of astrocytes was significantly reduced in MLD patient-derived neuronal cell populations (Fig. 5D, E). The defective cellular differentiation process may lead to a pathogenic mechanism of degenerative demyelination in the MLD brain.

There are some limitations of this study. We were not able to differentiate 100% pure MNs to elucidate protein expression related to mitochondrial dynamics, autophagy and quantification of sulfatide species. In our future studies, we will include different phenotypes of MLD, increasing the purity of differentiated MN to overcome the above issues. Additionally, single-cell physiology for mitochondrial dynamics and functional analysis of MNs will be considered.

5. Conclusion

We successfully generated iPSCs from MLD-derived SFs, followed by motor neuron progenitors and motor neurons. We detected lysosomal accumulation, autolysosome formation, mitochondrial fragmentation, impaired autophagy, mitophagy, UPR activation, and premature death in MNPs and MNs derived from MLD patients. Therefore, our
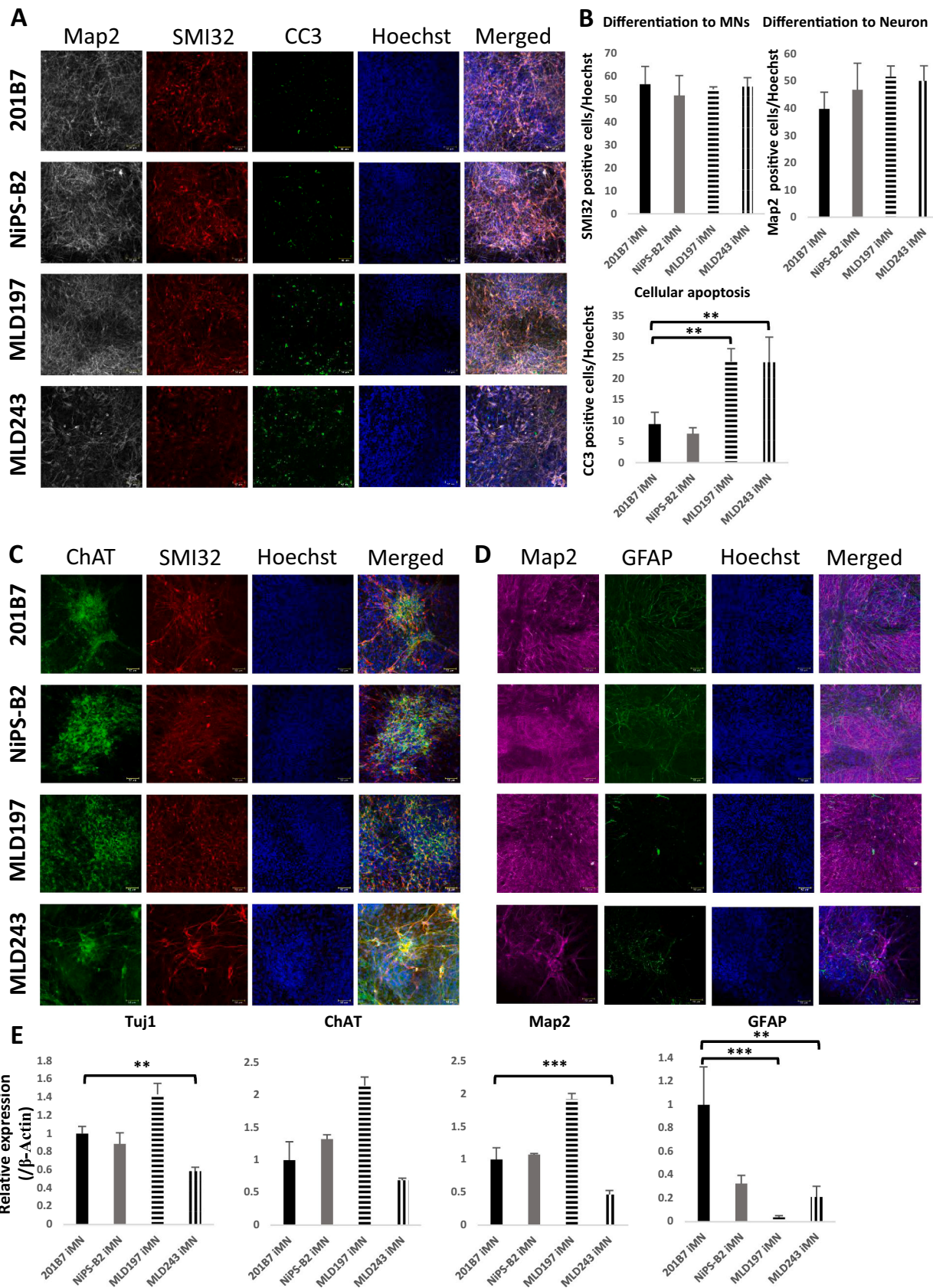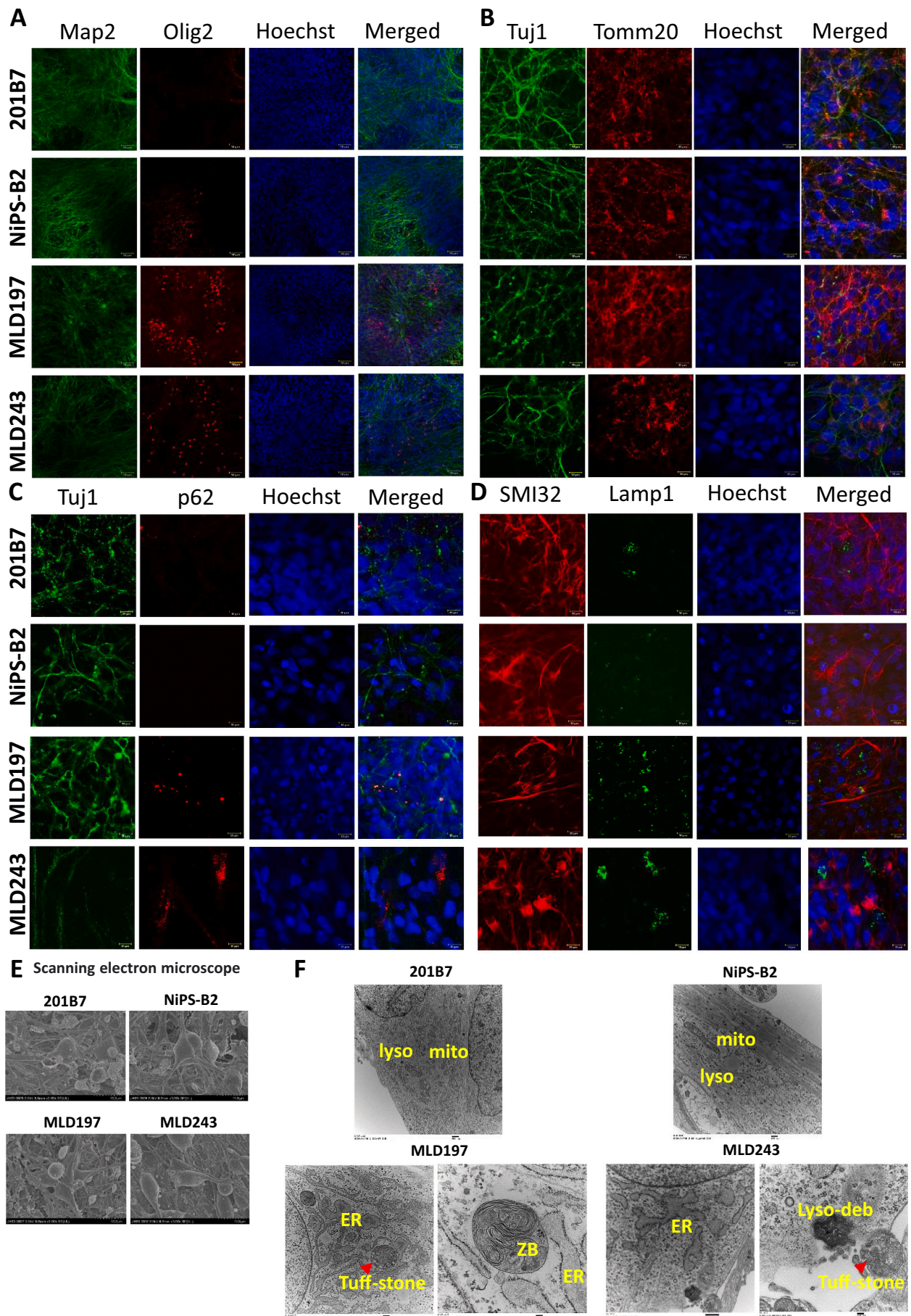
Fig. 5. Morphological and pathological characteristics of the MNs and associated cells. A. Detection of neurons. Mature neurons were detected by Map2, mature MNs were detected by SMI32, and apoptotic cells were detected by CC3. B. The calculation of detected cells shows a high number of apoptotic cells in patients compared with normal controls. C. Matured MNs are detected by SMI32 and ChAT. D. Mature astrocytes were detected by GFAP. E. Relative expression of neurons and astrocytes by qPCR. Each bar represents the mean ± SEM of three determinations. $*p < 0.05$, $**p < 0.01$, $***p < 0.005$ and $****p < 0.0001$.

(caption on next page)

Fig. 6. Morphological and pathological characteristics of the MNs. A. MNPs detected by Olig2 were found in large numbers in patient-derived cell populations after 28 days of differentiation. B. State of mitochondria. Aggregated and fragmented mitochondria have been shown to accumulate around patient-derived neuron nuclei. C. Observation of autophagy/mitophagy. Aberrant p62/SQSTM1 accumulation is shown in patient-derived neurons. D. Detection of lysosomes. Patient-derived neurons show enhanced LAMP1 both in the size of the lysosomes and area of each cell. E. SEM of neurons showed cells soma and cellular processes very clearly and having no morphological changes between normal and patients. F. Electron microscopy. Normal mitochondria, lysosomes, and no ER dilatation in normal neurons. However, patient-derived neurons show large lysosomal inclusions manifested as zebra bodies or tuff stones. The ER is massively dilated in MLD197 and MLD243 neurons.

neuropathological model of MLD could lead to new insights into its disease pathology and the discovery of novel drug targets.

Supplementary data to this article can be found online at https://doi.org/10.1016/j.ymgmr.2022.100852.

Contribution

MAH and MHO designed the research. MAH and YM performed the experiments and analyzed the data. MI supported the qPCR analysis and the statistics. MAH wrote the first draft of this paper and finalized the paper. YE and HJO directed the research, and YE acquired and organized the funding. CW, KS, JI, and TI provided logistic support. All the authors participated in the revision of the manuscript.

Declaration of Competing Interest

MAH is currently an employee of JCR Pharmaceuticals Co. Ltd. However, the work does not have any relation with the company, and the research was conducted before joining the industry. YE received research grants from Sanofi Co. and Actelion Pharmaceuticals. The other authors have no conflicts of interest to declare.

References

[1] T. Takahashi, T. Suzuki, Role of sulfatide in normal and pathological cells and tissues, J. Lipid Res. 53 (2012) 1437–1450.

[2] S. Xiao, C.V. Finkielstein, D.G.S. Capelluto, The enigmatic role of sulfatides: new insights into cellular functions and mechanisms of protein recognition, Adv. Exp. Med. Biol. 991 (2013) 27–40.

[3] J. Marcus, et al., Sulfatide is essential for the maintenance of CNS myelin and axon structure, Glia 53 (2006) 372–381.

[4] S. Grassi, et al., The role of 3-O-sulfogalactosylceramide, sulfatide, in the lateral organization of myelin membrane, Neurochem. Res. 41 (2016) 130–143.

[5] T. Ishibashi, et al., A myelin galactolipid, sulfatide, is essential for maintenance of ion channels on myelinated axon but not essential for initial cluster formation, J. Neurosci. 22 (2002) 6507–6514.

[6] V. Gieselmann, et al., Metachromatic leukodystrophy: molecular genetics and an animal model, J. Inherit. Metab. Dis. 21 (1998) 564–574.

[7] V. Gieselmann, I. Krägeloh-Mann, Metachromatic leukodystrophy—an update, Neuropediatrics 41 (2010) 1–6.

[8] D.F. van Rappard, J.J. Boelens, N.I. Wolf, Metachromatic leukodystrophy: disease spectrum and approaches for treatment, Best. Pract. Res. Clin. Endocrinol. Metab. 29 (2015) 261–273.

[9] M. Eckhardt, et al., Sulfatide storage in neurons causes hyperexcitability and axonal degeneration in a mouse model of metachromatic leukodystrophy, J. Neurosci. 27 (2007) 9009–9021.

[10] R. Van Zyl, V. Gieselmann, M. Eckhardt, Elevated sulfatide levels in neurons cause lethal audiogenic seizures in mice, J. Neurochem. 112 (2010) 282–295.

[11] S. Groeschel, et al., Cerebral grey and white matter changes and clinical course in metachromatic leukodystrophy, Neurology 79 (2012) 1662–1670.

[12] D. Wittke, D. Hartmann, V. Gieselmann, R. Lullmann-Rauch, Lysosomal sulfatide storage in the brain of arylsulfatase A-deficient mice: cellular alterations and topographic distribution, Acta Neuropathol. 108 (2004) 261–271.

[13] M. Molander-Melin, et al., Accumulation of sulfatide in neuronal and glial cells of arylsulfatase A deficient mice, J. Neurocytol. 33 (2004) 417–427.

[14] J.D. Malhotra, R.J. Kaufman, ER stress and its functional link to mitochondria: role in cell survival and death, Cold Spring Harb. Perspect. Biol. 3 (9) (2011), a004424.

[15] I.H. Park, et al., Disease-specific induced pluripotent stem cells, Cell 134 (2008) 877–886.

[16] F. Soldner, R. Jaenisch, iPSC diseasemodeling, Science 338 (2012) 1155–1156.

[17] M. Bellin, M.C. Marchetto, F.H. Gage, C.L. Mummery, Induced pluripotent stem cells: the new patient? Nat. Rev. Mol. Cell Biol. 13 (2012) 713–726.

[18] Y. Shi, H. Inoue, J.C. Wu, S. Yamanaka, Induced pluripotent stem cell technology: a decade of progress, Nat. Rev. 16 (2017) 116–130.

[19] J. Doerr, et al., Arylsulfatase A overexpressing human iPSC-derived neural cells reduce CNS sulfatide storage in a mouse model of metachromatic leukodystrophy, Mol. Ther. 23 (2015) 1519–1531.

[20] V. Meneghini, et al., Generation of human induced pluripotent stem cellderived bona fide neural stem cells for ex vivo gene therapy of metachromatic leukodystrophy, Stem Cells Transl. Med. 6 (2017) 352–368.

[21] G. Frati, M. Luciani, et al., Human iPSC-based models highlight defective glial and neuronal differentiation from neural progenitor cells in metachromatic leukodystrophy, Cell Death Dis. 9 (2018) 698.

[22] a. K.P. Kim, J. Yoon, J. Kim, A. Röpke, B. Shin, et al., Generation of a human iPSC line (MPIi007-A) from a patient with Metachromatic leukodystrophy, Stem Cell Res. 48 (2020), 101993;
b. S. Regis, F. Corsolini, M. Stroppiano, R. Cusano, M. Filocamo, Contribution of arylsulfatase A mutations located on the same allele to enzyme activity reduction and metachromatic leukodystrophy severity, Hum. Genet. 110 (2002) 351–355;
c. A. Polten, A.L. Fluharty, C.B. Fluharty, J. Kappler, K. von Figura, V. Gieselmann, Molecular basis of different forms of metachromatic leukodystrophy, N. Engl. J. Med. 324 (1991) 18–22.

[23] R. Saito, T. Miyajima, T. Iwamoto, C. Wu, K. Suzuki, et al., A neuropathological cell model derived from Niemann−Pick disease type C patient-specific iPSCs shows disruption of the p62/SQSTM1−KEAP1−NRF2 Axis and impaired formation of neuronal networks, Mol. Gen. Meta Rep. 28 (2021), 100784.

[24] K. Okita, Y. Matsumura, et al., A more efficient method to generate integration-free human iPS cells, Nat. Methods 8 (2011) 409–412.

[25] K. Nishimura, M. Ohtaka, et al., Simple and effective generation of transgene-free induced pluripotent stem cells using an auto-erasable Sendai virus vector responding to microRNA-302, Stem Cell Res 23 (2017) 13–19.

[26] M. Nakagawa, Y. Taniguchi, S. Senda, et al., A novel efficient feeder-free culture system for the derivation of human induced pluripotent stem cells, Sci. Rep. 4 (2014) 3594.

[27] Y. Okada, A. Matsumoto, T. Shimazaki, R. Enoki, A. Koizumi, S. Ishii, Y. Itoyama, G. Sobue, H. Okano, Spatiotemporal recapitulation of central nervous system development by murine embryonic stem cell-derived neural stem/progenitor cells, Stem Cells 26 (2008) 3086–3098.

[28] N. Ichiyanagi, K. Fujimori, M. Yano, C. Ishihara-Fujisaki, T. Sone, et al., Establishment of in vitro FUS-associated familial amyotrophic lateral sclerosis model using human induced pluripotent stem cells, Stem Cell Rep. 6 (2016) 496–510.

[29] A. Lattanzi, M. Neri, C. Maderna, I. di Girolamo, S. Martino, et al., Widespread enzymatic correction of CNS tissues by a single intracerebral injection of therapeutic lentiviral vector in leukodystrophy mouse models, Hum. Mol. Genet. 19 (2010) 2208–2227.

[30] J. Tolar, et al., Hematopoietic differentiation of induced pluripotent stem cells from patients with mucopolysaccharidosis type I (Hurler syndrome), Blood 117 (2010) 839–847.

[31] T. Lemonnier, et al., Modeling neuronal defects associated with a lysosomal disorder using patient-derived induced pluripotent stem cells, Hum. Mol. Genet. 20 (2011) 3653–3666.

[32] I. Canals, et al., Activity and high-order effective connectivity alterations in sanfilippo C patient-specific neuronal networks, Stem Cell Rep. 5 (2015) 546–557.

[33] L.M. Panicker, et al., Induced pluripotent stem cell model recapitulates pathologic hallmarks of Gaucher disease, Proc. Natl. Acad. Sci. U. S. A. 109 (2012) 18054–18059.

[34] G. Tiscornia, et al., Neuronopathic Gaucher's disease: induced pluripotent stem cells for disease modelling and testing chaperone activity of small compounds, Hum. Mol. Genet. 22 (2013) 633–645.

[35] Y. Sun, et al., Properties of neurons derived from induced pluripotent stem cells of Gaucher disease type 2 patient fibroblasts: potential role in neuropathology, PLoS One 10 (2015), e0118771.

[36] O. Awad, et al., Altered TFEB-mediated lysosomal biogenesis in Gaucher disease iPSC-derived neuronal cells, Hum. Mol. Genet. 24 (2015) 5775–5788.

[37] M.-Y. Son, et al., A novel human model of the neurodegenerative disease GM1 gangliosidosis using induced pluripotent stem cells demonstrates inflammasome activation, J. Pathol. 237 (2015) 98–110.

[38] X. Lojewski, et al., Human iPSC models of neuronal ceroid lipofuscinosis capture distinct effects of TPP1 and CLN3 mutations on the endocytic pathway, Hum. Mol. Genet. 23 (2014) 2005–2022.

[39] H. Wei, S.J. Kim, Z. Zhang, P.C. Tsai, K.E. Wisniewski, A.B. Mukherjee, ER and oxidative stresses are common mediators of apoptosis in both neurodegenerative and non-neurodegenerative lysosomal storage disorders and are alleviated by chemical chaperones, Hum. Mol. Genet. 17 (2008) 469–477.

[40] A. Tessitore, M.P. del Martin, R. Sano, Y. Ma, L. Mann, A. Ingrassia, et al., GM1-ganglioside-mediated activation of the unfolded protein response causes neuronal death in a neurodegenerative gangliosidosis, Mol. Cell. 15 (2004) 753–766.

[41] Z. Zhang, Y.C. Lee, S.J. Kim, M.S. Choi, P.C. Tsai, Y. Xu, et al., Palmitoyl-protein thioesterase-1 deficiency mediates the activation of the unfolded protein response and neuronal apoptosis in INCL, Hum. Mol. Genet. 15 (2006) 337–346.

[42] G.R. Villani, A. Chierchia, D. Di Napoli, P. Di Natale, Unfolded protein response is not activated in the mucopolysaccharidoses but protein disulfide isomerase 5 is deregulated, J. Inherit. Metab. Dis. 35 (2012) 479–493.

[43] T. Suzuki, M. Shimoda, K. Ito, S. Hanai, H. Aizawa, T. Kato, et al., Expression of human Gaucher disease gene GBA generates neurodevelopmental defects and ER stress in Drosophila eye, PLoS One 8 (2006), e69147.

[44] J. Kobolak, K. Molnar, E. Varga, I. Bock, B. Jezso, et al., Modelling the neuropathology of lysosomal storage disorders through disease-specific human induced pluripotent stem cells, Exp. Cell Res. 380 (2019) 216–233.

[45] K. Irahara-Miyana, T. Otomo, H. Kondo, M.A. Hossain, et al., Unfolded protein response is activated in Krabbe disease in a manner dependent on the mutation type, J. Hum. Genet. 63 (2018) 699–706.

[46] H. Lee, Y. Yoon, Mitochondrial fission and fusion, Biochem. Soc. Trans. 44 (2016) 1725–1735.

[47] Y. Chen, L. Yan, et al., The role of DRP1 in ropivacaine-induced mitochondrial dysfunction and neurotoxicity, Artif. Cells Nanomed. Biotechnol. 47 (2019) 1788–1796.

[48] K. Kiselyov, J.J.J. Jennigs, Y. Rbaibi, C.T.X. Chu, Autophagy, mitochondria, and cell death in lysosomal storage diseases, Autophagy 3 (3) (2007) 259–262.

[49] Du, Z.W., Chen, H., Liu, H., Lu, J., Qian, K. et al. Generation and expansion of highly pure motor neuron progenitors from human pluripotent stem cells. Nat. Commun. 6, 6626.

[50] Z.B. Gaber, B.G. Novitch, All the embryo's a stage, and Olig2 in its time plays many parts, Neuron 69 (2011) 833–835.

[51] A. Buffo, M.R. Vosko, D. Ertürk, G.F. Hamann, M. Jucker, Expression pattern of the transcription factor Olig2 in response to brain injuries: implications for neuronal repair, Proc. Natl. Acad. Sci. U. S. A. 102 (2005) 18183–18188.

[52] C.S. von Bartheld, J. Bahney, S. Herculano-Houzel, The search for true numbers of neurons and glial cells in the human brain: a review of 150 years of cell counting, J. Comp. Neurol. 524 (2016) 3865–3895.

[53] C.M. Willis, A.M. Nicaise, E.R. Bongarzone, M. Givogri, Astrocyte support for oligodendrocyte differentiation can be conveyed via extracellular vesicles but diminishes with age, Sci. Rep. 10 (2020) 828.